Materials Research Bulletin 74 (2016) 169–176

Contents lists available at ScienceDirect

Materials Research Bulletin

journal homepage: www.elsevier.com/locate/matresbu

Low dimensional magnetism in $MnNb_{2-x}V_xO_6$

M.L. Hneda[a,b,c,*], J.B.M. da Cunha[a], M.A.C. Gusmão[a], O. Isnard[b,c]

[a] Universidade Federal do Rio Grande do Sul, Porto Alegre, Brazil
[b] Institut Néel/CNRS, Grenoble, France
[c] Université Joseph Fourier, Grenoble, France

ARTICLE INFO

Article history:
Received 31 July 2015
Accepted 14 October 2015
Available online 20 October 2015

Keywords:
A. Oxides
B. Magnetic properties
B. Magnetic structure
C. X-ray diffraction
C. Neutron diffraction

ABSTRACT

The structural and magnetic properties of $MnNb_{2-x}V_xO_6$ samples were studied. These materials belong to the AB_2O_6 class, which presents low-dimensional magnetism. Curie-Weiss fitting gives a negative Weiss temperature that is a characteristic of dominant antiferromagnetic interactions in paramagnetic region. Rietveld refinements of neutron diffraction data show that magnetic moments are aligned antiferromagnetically within the zig-zag chains running along the *c* axis. Unlike other ANb_2O_6 type systems crystallizing also in *Pbcn* space group and presenting ferromagnetic Ising chains, $MnNb_{2-x}V_xO_6$ samples exhibit antiferromagnetic type order along the chains. At 1.5 K, the Mn atoms are found to carry an ordered magnetic moment of about 4.3 μ_B. The Mn chains are antiferromagnetic and do not present significant anisotropy. These characteristics and the high spin allowed us to model the system as weakly interacting classical Heisenberg chains, estimating the values of both intra- and interchain exchange constants evolution with *x* content.

1. Introduction

The system AB_2O_6 has been extensively studied because of interesting photoluminescence [1], dielectric [2,3], and magnetic properties [4–6]. In these compounds *A* is a divalent magnetic cation (Fe, Co, Cr, Ni, Cu, Mn, . . .) and *B* a non-magnetic pentavalent cation. The crystal structure depends strongly on the *B* ion. For example, *B* = Ta yields a tetragonal structure [4] while Nb favors an orthorhombic one [5,7], with the exception of $CuNb_2O_6$ which presents a monoclinic structure [8]. Monoclinic and triclinic structures are generally observed with *B*=V [9,10]. Fig. 1 shows the crystal structure of $MnNb_2O_6$, highlighting the oxygen octahedra surrounding Mn ions. The structure can be viewed as a stacking of slightly tilted oxygen octahedra, forming zig-zag chains along the *c* axis. Such zig-zag chains are also characteristic of the α-PbO_2 structure [11,12].

The ANb_2O_6 phases usually exhibit weakly interacting one-dimensional magnetic chains [5,13,14]. $MnNb_2O_6$ was found to undergo a transition from a paramagnetic phase to an ordered structure [7,15,16] at 4.40 K.

We have recently reported [4,17–19] results on the ANb_2O_6 and ATa_2O_6 series of compounds, characterized by 1D and 2D magnetic behavior, respectively. In this work we present a detailed investigation of $MnNb_{2-x}V_xO_6$ (*x* = 0, 0.1, 0.2, 0.3 and 0.4) by means of magnetic measurements, powder neutron and X-ray diffraction, and specific-heat measurements. This study is aimed to investigate the effect of substitution on the structural and magnetic properties of the $MnNb_{2-x}V_xO_6$ series of compounds in particular the influence on the intra and interchain exchange interactions and its consequence on the magnetic structure.

2. Experimental details

Samples were prepared with appropriate amounts of Mn acetate ($C_4H_6MnO_4{\cdot}4H_2O$), V_2O_5 and Nb_2O_5. The mixtures were ground, pressed into pellets, and heat-treated at 400, 650 and 725 °C for 12, 16 and 48 h, respectively. All these heat treatments were interspersed with grinding processes. $MnNb_2O_6$ was subject to another treatment at 1100 °C for 36 h, while the $MnNb_{2-x}V_xO_6$ samples (*x* = 0.1, 0.2, 0.3 and 0.4) where further treated at 725 °C for 48 h. The heat treatment at 725 °C was necessary to avoid evaporation of the precursor V_2O_5. This was done to ensure a unique phase, and immediately followed by a quenching process.

Sample purity was first checked by X-ray diffraction (XRD) analysis followed by neutron diffraction (ND) and magnetic measurements. The XRD was performed in Bragg–Brentano geometry, using Cu $K\alpha$ radiation, $\lambda(K\alpha1) = 1.540562$ Å and $\lambda(K\alpha2) = 1.544390$ Å, with a scan step of 0.05° and angular 2θ range from 10° to 90°.

* Corresponding author at: Universidade Federal do Rio Grande do Sul, Porto Alegre, Brazil. Fax: +55 (51) 3308-7286.
E-mail address: mlhneda@if.ufrgs.br (M.L. Hneda).

http://dx.doi.org/10.1016/j.materresbull.2015.10.030
0025-5408/

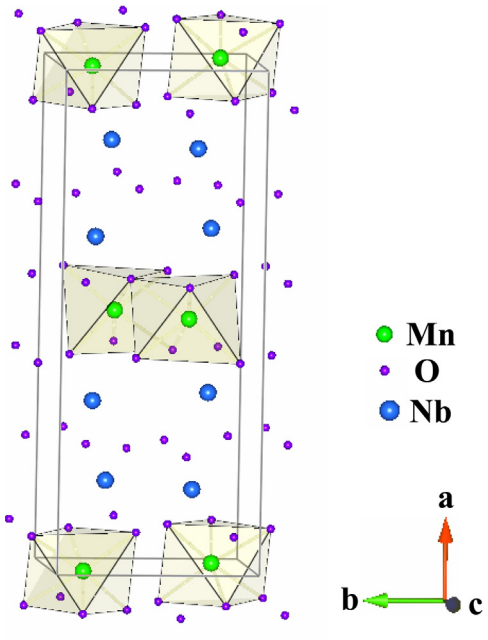

Fig. 1. Crystal structure of the $MnNb_2O_6$ compound, showing the oxygen octahedra surrounding the Mn atoms.

ND patterns were recorded with the double-axis high-flux diffractometer D1B operated by the CNRS at the Institut Laue Langevin (ILL), Grenoble, using a 2.52 Å wavelength selected by a pyrolytic graphite monochromator. D1B is a powder diffractometer operating with a take-off angle of the monochromator of 44° (in 2θ). In this configuration the multicounter is composed of 1280 cells covering a total angular domain of 128° (in 2θ), with a detector step of 0.1°. A vanadium sample holder was used. Neutron measurements have been carried out down to 1.5 K by pumping on the He liquid.

Rietveld refinement with FullProf package [20] was used for XRD and ND data to extract the crystallographic and magnetic parameters. Agreement factors used in this paper are defined according to the guidelines of the Rietveld refinement [21].

Magnetic measurements were undertaken on powder samples in the temperature range from 1.9 to 300 K, using an extraction magnetometer. Isothermal magnetization curves were recorded in applied magnetic fields ranging from $\mu_0 H = 0$ to 10 *T*, and the thermal dependence of magnetic susceptibility was measured in a field of $\mu_0 H = 0.5$ *T*.

Specific heat measurements were performed on pellets (mass ~5 mg), in the range of 1.8–300 K, using a PPMS (Physical Property Measurement System—Quantum Design) with the temperature relaxation method. It consists in increasing the sample temperature with a known power and then fitting the temperature relaxation during heating and cooling.

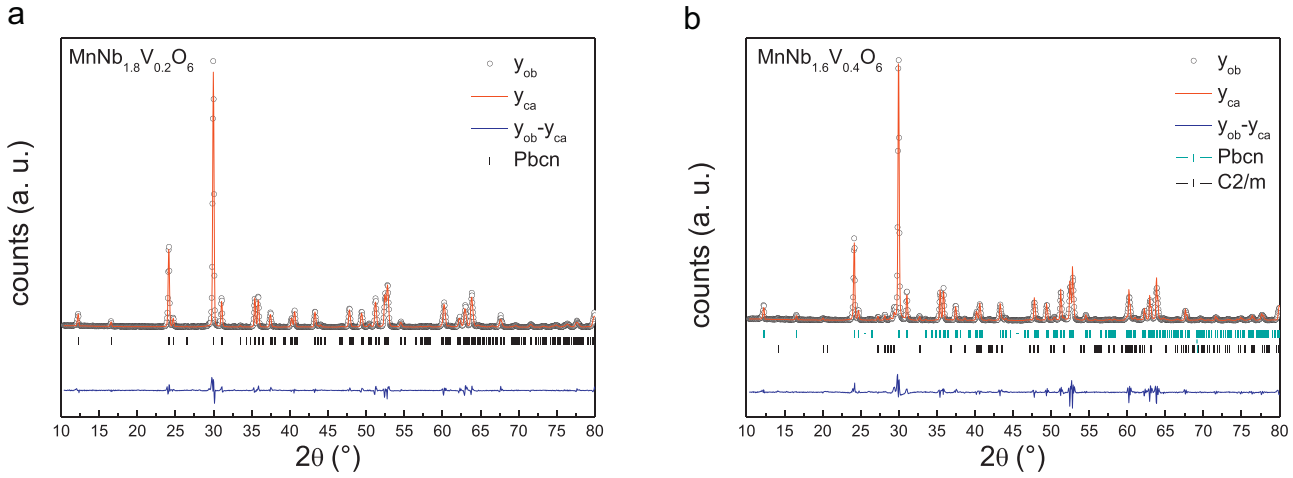

Fig. 2. Rietveld refinement of the X-ray diffraction pattern recorded at room temperature for $x = 0.2$ and 0.4. The Bragg positions correspond to the *Pbcn* and *C2/m* space groups, as indicated.

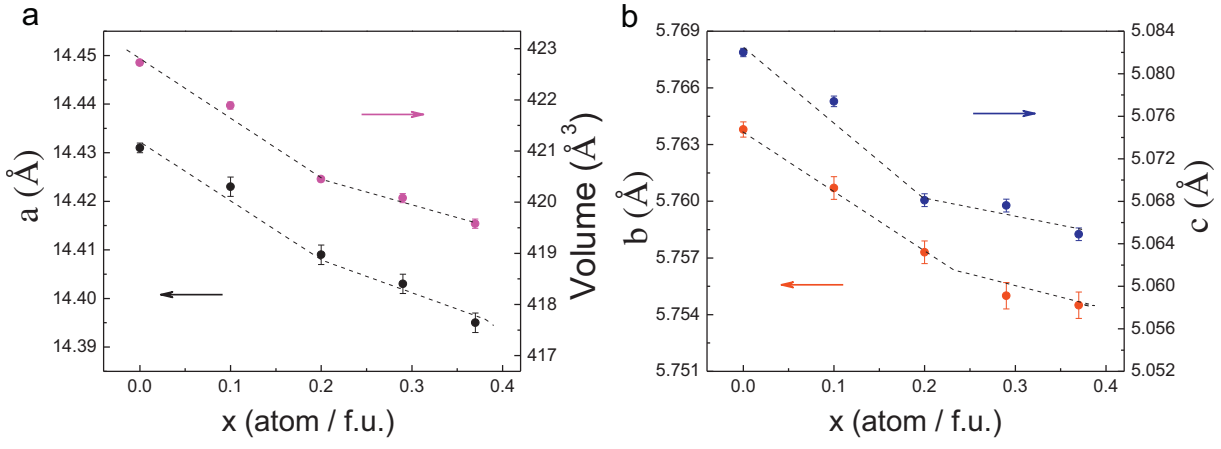

Fig. 3. Concentration dependence of the unit-cell parameters of the $MnNb_{2-x}V_xO_6$ compounds at room temperature. The lines are guide for the eyes.

Table 1
XRD parameters at room temperature for $MnNb_{2-x}V_xO_6$ (*Pbcn*) compounds.

		$MnNb_2O_6$	$MnNb_{1.9}V_{0.1}O_6$	$MnNb_{1.8}V_{0.2}O_6$
Mn	*x*	0	0	0
	y	0.180(3)	0.176(4)	0.178(3)
	z	0.25	0.25	0.25
Nb/V	*x*	0.1626(3)	0.1630(4)	0.1630(4)
	y	0.3188(9)	0.3182(1)	0.318(1)
	z	0.760(2)	0.758(2)	0.757(2)
O1	*x*	0.102(2)	0.098(2)	0.098(2)
	y	0.412(5)	0.411(6)	0.414(6)
	z	0.445(7)	0.462(9)	0.454(9)
O2	*x*	0.083(2)	0.085(2)	0.083(2)
	y	0.127(6)	0.137(7)	0.133(7)
	z	0.888(7)	0.890(8)	0.886(8)
O3	*x*	0.253(3)	0.254(3)	0.252(3)
	y	0.127(6)	0.129(8)	0.130(6)
	z	0.586(6)	0.598(9)	0.589(8)
a (Å)		14.431(1)	14.423(2)	14.409(2)
b (Å)		5.7638(4)	5.7607(6)	5.7573(6)
c (Å)		5.0820(4)	5.0774(5)	5.0681(6)
Volume (Å^3)		422.73(5)	421.89(7)	420.45(5)
R_{WP} (%)		15.2	18.4	17.2
R_B (%)		4.8	5.8	6.2

3. Results and discussion

3.1. X-ray diffraction

From XRD-pattern analysis we observe that all the $MnNb_{2-x}V_xO_6$ samples (with *x* varying in the range *x* = 0–0.2) present a single phase, with the *Pbcn* space-group symmetry. Rietveld analysis of the XRD patterns recorded at room temperature for *x* = 0.2 and 0.4 are shown in Fig. 2. For the *x* = 0.2 we observe only orthorhombic *Pbcn*. In contrast, for *x* = 0.4 it is possible to observe a small amount of a monoclinic *C2/m* phase. The $MnNb_{1.7}V_{0.3}O_6$ sample presented 97% of *Pbcn* and 3% of *C2/m*, while $MnNb_{1.6}V_{0.4}O_6$ showed 95% of *Pbcn* and 5% of *C2/m*. The lattice-parameter variation of orthorhombic *Pbcn* as function of *x* is show in Fig. 3. An anisotropic contraction (related to *x* = 0) was observed in the cell parameters: $\Delta a/a = -0.00247$, $\Delta b/b = -0.00162$ and $\Delta c/c = -0.00336$.

Table 1 shows the room temperature XRD parameters for $MnNb_{2-x}V_xO_6$ compounds: atomic position, cell parameters and agreement Rietveld factors like R_{WP} and R_B.

Table 2
Néel temperature, Curie–Weiss temperature, Curie constant and effective magnetic moment of $MnNb_{2-x}V_xO_6$ compounds obtained from measurements of dc susceptibility.

	T_N (K)	θ_{CW} (K)	*C* (emuK/molOe)	μ_{eff} (μ_B)
$MnNb_2O_6$	4.40	−24.5	4.78	6.18
$MnNb_{1.9}V_{0.1}O_6$	4.64	−25.0	4.66	6.11
$MnNb_{1.8}V_{0.2}O_6$	4.68	−25.5	4.68	6.12

3.2. Magnetic measurements

The temperature dependence of the dc susceptibility for $MnNb_2O_6$ sample recorded at $\mu_0 H = 0.5\,T$ is shown in Fig. 4. Looking closely around the observed peak, one sees that it is not sharp, but rather broad, and the Néel temperature corresponds to an inflection point slightly below the maximum. This means that the compound exhibits characteristic features of low-dimensional magnetism, similarly to what was observed in other ANb_2O_6 compounds [5,13,14,17–19]. According to Fisher [22] in low-dimensional systems the magnetic contribution to the specific heat is directly related to $\partial(T\chi)/\partial T$. The behavior of this derivative is shown in the inset of Fig. 4 for *x* = 0 and 0.2, where one sees that the curves exhibit a peak at the ordering temperature. The values of Néel temperature so determined are about 4.6 K (see also Table 2).

The paramagnetic susceptibility as a function of temperature were fitted to the Curie-Weiss law, $\chi(T) = C/(T - \theta_{CW})$ for temperatures above the ordering temperature. The Table 2 shows the

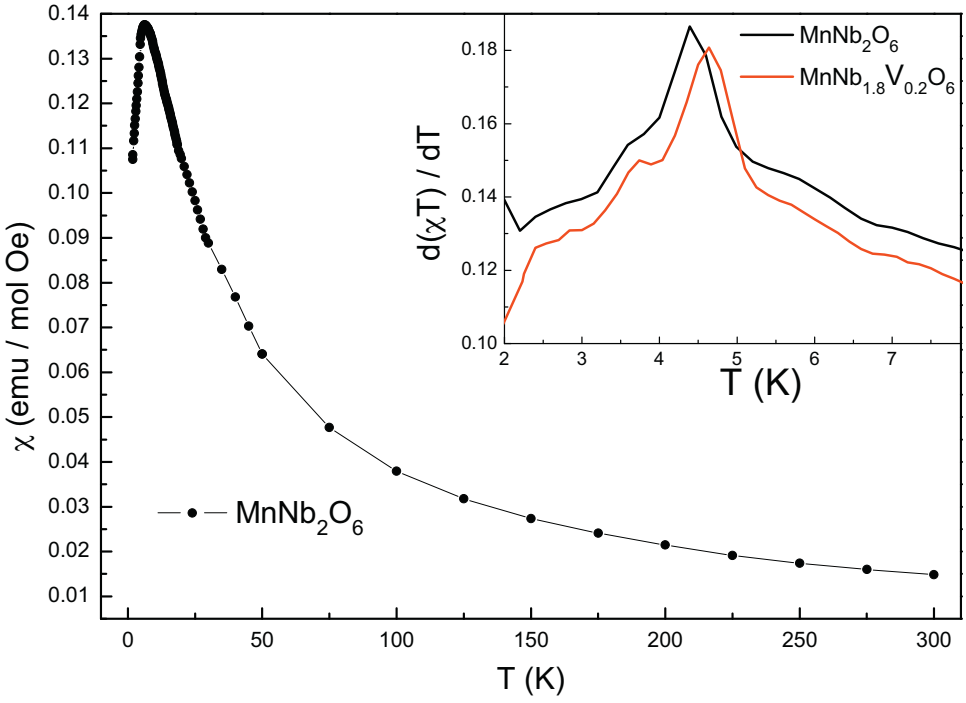

Fig. 4. Temperature dependence of the dc susceptibility recorded at $\mu_0 H = 0.5\,T$ for $MnNb_2O_6$ sample. The inset shows the $\partial(T\chi)/\partial T$ for *x* = 0 and 0.2.

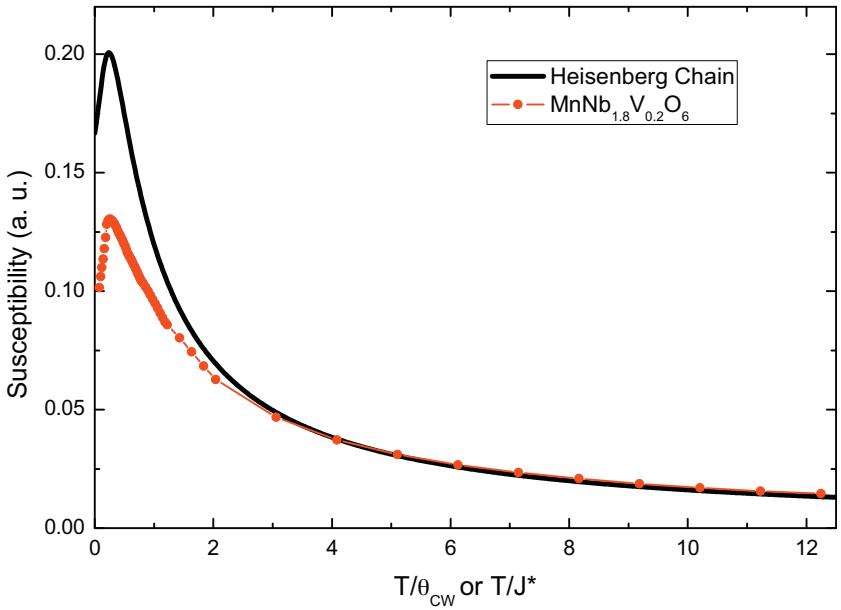

Fig. 5. Comparative plot of the susceptibility data as a function of temperature for $MnNb_{1.8}V_{0.2}O_6$ and the exact result for a classical AF Heisenberg chain. The temperature scaled by the Curie–Weiss θ_{CW} for the experimental data and by the rescaled exchange $J^* = 4S^2J$ for the theoretical curve.

parameters obtained from this analysis, for the samples $x = 0$–0.2. The effective magnetic moment in the paramagnetic state has been derived from the Curie constant by [9].

In $MnNb_2O_6$, Mn^{2+} cations have electronic state $^6S_{5/2}$. The calculated value of effective magnetic moment, given by $\mu_{eff} = g\,\mu_B[S(S+1)]^{1/2}$ [7,23], is 5.92 μ_B for $g = 2$ and $S = 5/2$. This value is close to the one obtained from susceptibility measurements, as can be seen in Table 2. This confirms the divalent state of Mn in the studied compound. It also shows that orbital effects are essentially absent, and Ising-like behavior due to strong anisotropy, as observed for Co and Fe [17,19], should not be expected. Nevertheless, the slightly higher Mn effective moment implies that the angular contribution is not strictly zero. The values shown in Table 2 are in agreement with those reported in Ref. [24] for $MnNb_2O_6$ ($\theta_{CW} = -20{\cdot}5$ K, $C = 4.37$ emu K/mol Oe, and $\mu_{eff} = 5.91\ \mu_B$).

Table 3
Exchange parameters for the three indicated compositions, as obtained from comparisons between the experimental susceptibility and the exact result for a classical Heisenberg chain.

	J/k_B (K)	J'/k_B (K)
$MnNb_2O_6$	−1.09	−0.365
$MnNb_{1.9}V_{0.1}O_6$	−1.07	−0.358
$MnNb_{1.8}V_{0.2}O_6$	−1.05	−0.350

Taking into account the presence of spin chains, which are weakly interacting judging from the low values of T_N compared to θ_{CW}, and the high spin value ($S = 5/2$), we can envisage an analysis based on the classical Heisenberg chain. An exact expression for the susceptibility of such a chain was obtained by Fisher [25]. It corresponds to the limit $S \rightarrow$ infinite, in which the spins are replaced by classical vectors of unit length and the exchange

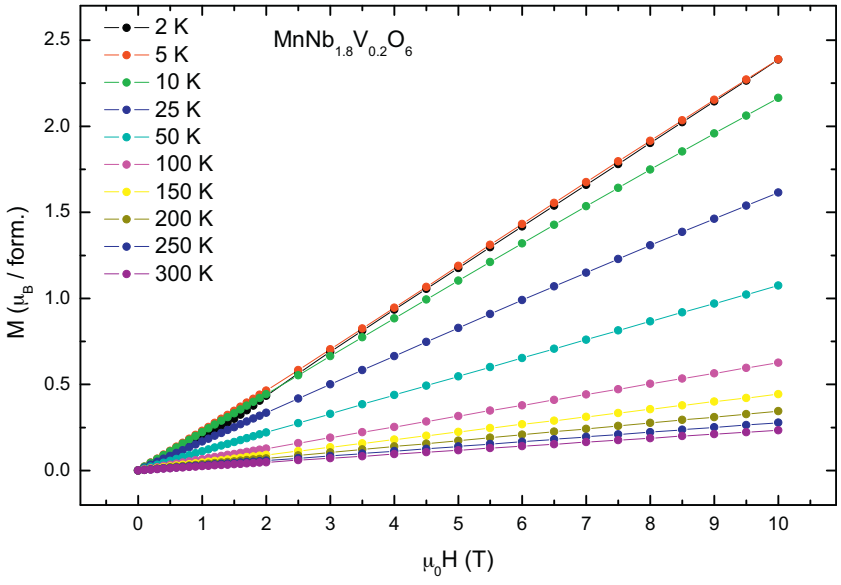

Fig. 6. Isothermal magnetization curves recorded at the indicated temperatures for the $MnNb_{1.8}V_{0.2}O_6$ compound.

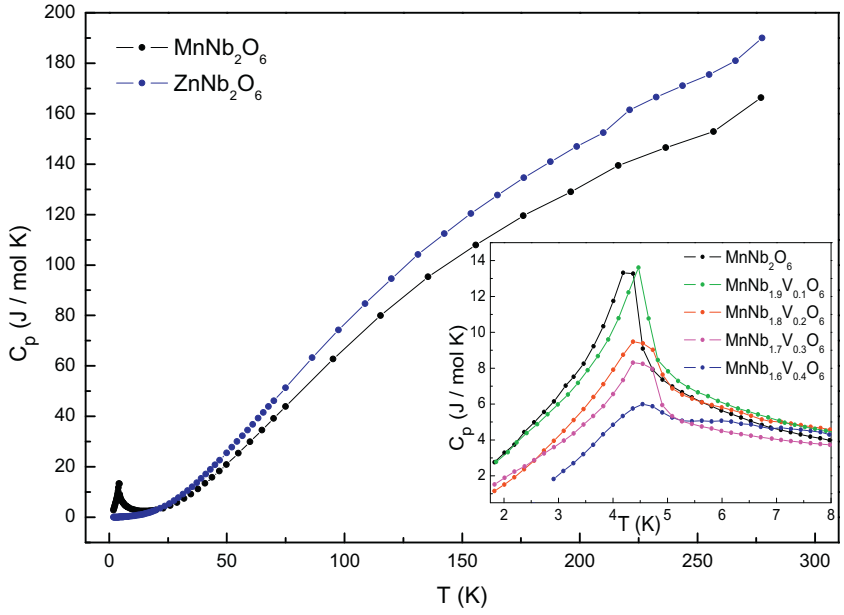

Fig. 7. Specific-heat behavior of $MnNb_2O_6$ and $ZnNb_2O_6$ (non-magnetic). The inset shows a detailed view of the region near the Néel temperature for $MnNb_{2-x}V_xO_6$ samples.

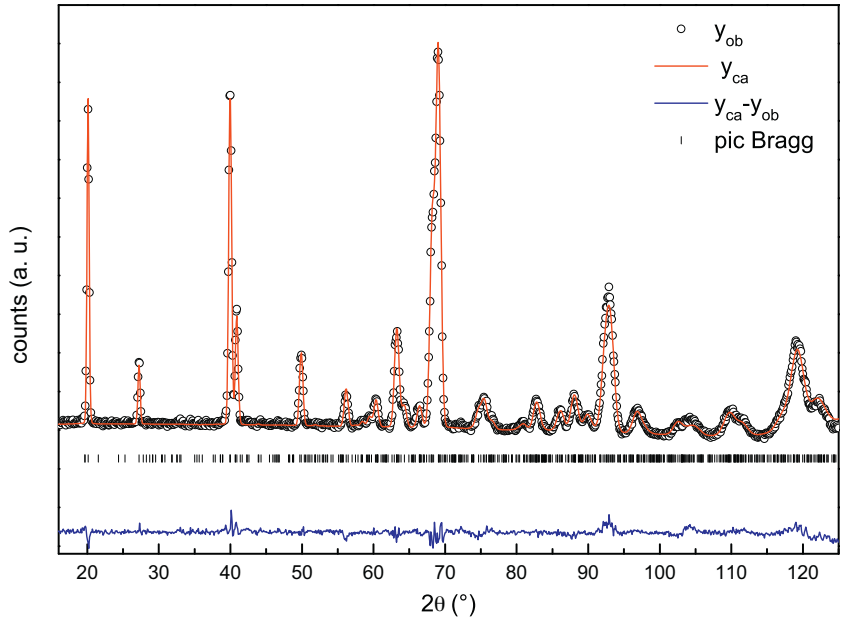

Fig. 8. Rietveld refinement of neutron-diffraction pattern recorded at 280 K for $MnNb_2O_6$. The Bragg positions correspond to the *Pbcn* space group.

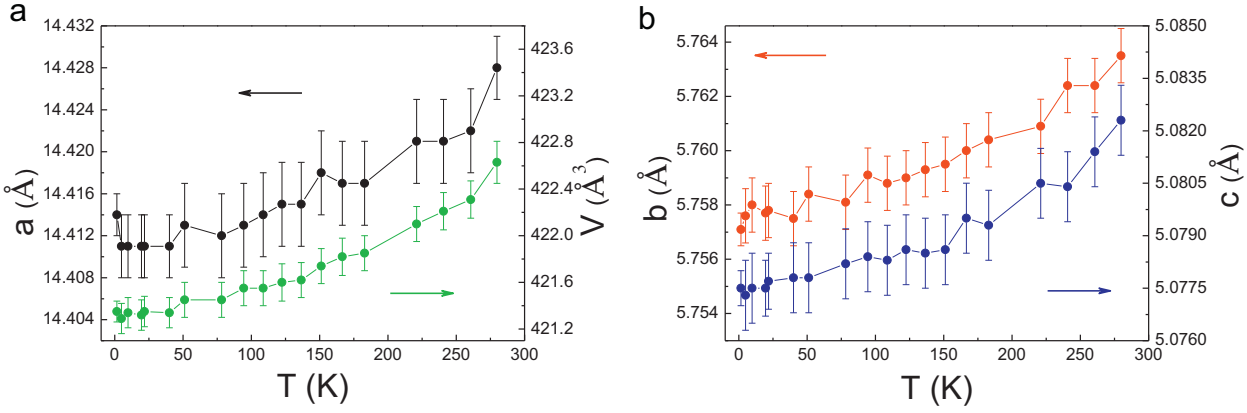

Fig. 9. Temperature dependence of unit-cell parameters for $MnNb_2O_6$ (1.5–280 K). Values were obtained from Rietveld refinement of ND patterns.

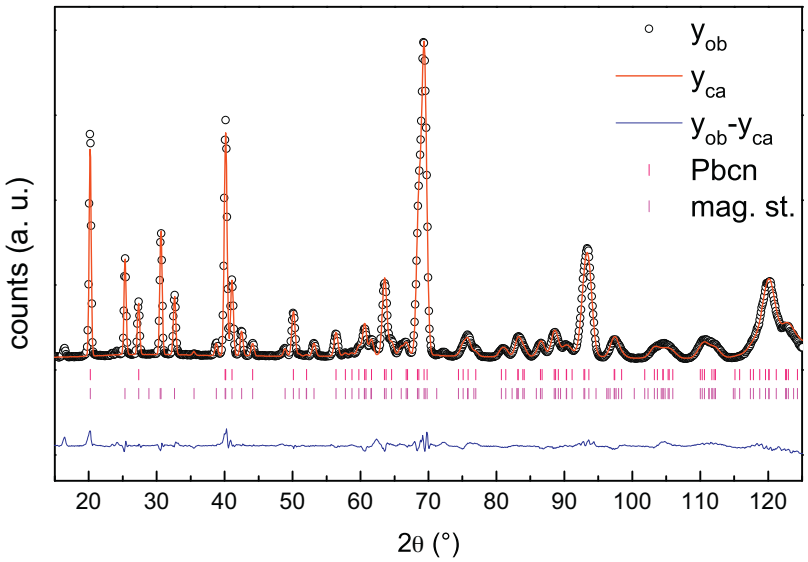

Fig. 10. Rietveld refinement of the ND pattern recorded at 1.5 K for $MnNb_{1.8}V_{0.2}O_6$. The first and second rows of markers refer to Bragg-peak positions corresponding to the nuclear contribution (*Pbcn* space group) and to the magnetic contribution, respectively.

interaction J along the chain is rescaled to $J^* = 4S^2J$. In Fig. 5 we plot the classical AF chain's susceptibility as a function of $T/|J^*|$. The same plot includes the experimental data for $MnNb_{1.8}V_{0.2}O_6$ as a function of $T/|\theta_{CW}|$. It is clear that the physics of the classical chain plays an important role in this system, although the deviations seen in Fig. 5 reflect the interchain interactions and possibly the quantum nature of the spins.

From Ref. [25] we know that the susceptibility maximum is located at $T/|J^*| = 0.2382$. By supposing that the experimental maximum coincides with the classical-chain limit, we directly relate J^* to θ_{CW} from the plots in Fig. 5, which allows to determine the intrachain exchange J from its relation to J^* and from the obtained values of θ_{CW} (Table 2). On the other hand, we have the exact relation $\theta_{CW} = 2\ (2J + 6J')\ S(S+1)/3$, where J' is the average exchange interaction between a given spin and those closest to it in the six neighboring chains. From this we are able to estimate both exchange constants, whose values are listed in Table 3 for the three samples studied here. Despite the differences being small, there is

Table 4
Structural parameters obtained from Rietveld refinement of the ND pattern recorded at the indicated temperatures for $MnNb_{2-x}V_xO_6$ compounds.

		$MnNb_2O_6$		$MnNb_{1.9}V_{0.1}O_6$		$MnNb_{1.8}V_{0.2}O_6$	
Temp. →		280 K	1.5 K	200 K	1.5 K	9.7 K	1.5 K
Mn	*x*	0	0	0	0	0	0
	y	0.186(4)	0.165(3)	0.179(6)	0.179(3)	0.184(4)	0.182(3)
	z	0.25	0.25	0.25	0.25	0.25	0.25
Nb/V	*x*	0.1605(5)	0.1600(4)	0.1597(7)	0.1600(6)	0.1602(6)	0.1603(6)
	y	0.316(2)	0.315(1)	0.311(2)	0.31(2)	0.312(2)	0.312(1)
	z	0.763(3)	0.763(2)	0.760(4)	0.761(3)	0.758(3)	0.758(3)
O1	*x*	0.0945(7)	0.0954(6)	0.0947(9)	0.0951(8)	0.0956(7)	0.0964(7)
	y	0.394(2)	0.400(2)	0.399(3)	0.398(3)	0.396(3)	0.397(3)
	z	0.434(2)	0.438(2)	0.439(3)	0.437(3)	0.439(3)	0.439(3)
O2	*x*	0.0803(7)	0.0817(6)	0.0829(9)	0.0819(8)	0.0833(7)	0.0830(7)
	y	0.107(2)	0.109(2)	0.106(3)	0.109(3)	0.112(2)	0.113(2)
	z	0.907(3)	0.902(2)	0.900(3)	0.903(3)	0.899(3)	0.900(3)
O3	*x*	0.2577(9)	0.2541(7)	0.2532(1)	0.2532(1)	0.2541(9)	0.2529(9)
	y	0.128(2)	0.128(2)	0.125(3)	0.125(2)	0.128(2)	0.127(2)
	z	0.586(3)	0.585(2)	0.581(4)	0.582(3)	0.582(3)	0.585(3)
a (Å)		14.428(2)	14.414(2)	14.386(4)	14.391(3)	14.362(3)	14.371(3)
b (Å)		5.7635(1)	5.7571(6)	5.749(1)	5.7504(9)	5.7431(9)	5.7452(9)
c (Å)		5.0823(1)	5.0775(5)	5.068(1)	5.0690(8)	5.0574(8)	5.0594(7)
Volume (Å^3)		422.6(2)	421.35(9)	419.2(2)	419.4(1)	417.1(1)	417.7(1)
R_{WP} (%)		5.3	4.5	9.2	7.9	7.8	7.9
R_B (%)		7.2	6.4	10.5	8.2	8.0	7.3
R_M (%)		–	9.4	–	11.2	–	9.3
μ (μ_B)		–	4.13(6)	–	4.30(9)	–	4.28(8)
θ (°)		–	71.3	–	70.4	–	71.6
φ (°)		–	10.4	–	4.0	–	1.6

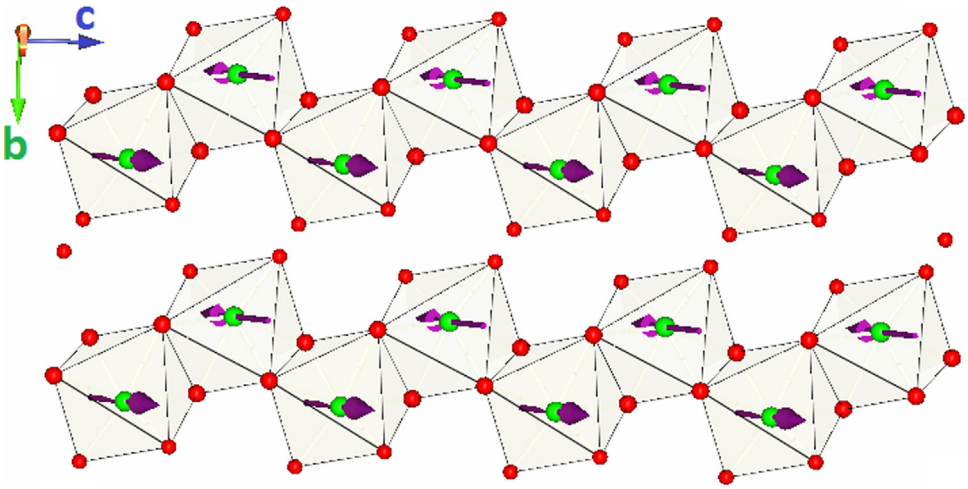

Fig. 11. Antiferromagnetic zig-zag chain formed by Mn octahedra along the *c* axis for $MnNb_{2-x}V_xO_6$ samples.

a consistent reduction of the interactions as substitution of V for Nb increases. This is more noticeable in the interchain coupling J', which can be understood by the location of (Nb,V) planes separating the chains along the *a* direction (see Fig. 1). It is noteworthy that the negative sign of the J' exchange constant found between the chains is confirming the hypothesis of an antiferromagnetic coupling leading to frustration on the pseudo triangular net of Mn chains.

Fig. 6 shows isothermal magnetization curves recorded at the indicated temperatures for the $MnNb_{1.8}V_{0.2}O_6$ compound. The behavior is typical of antiferromagnetic ordering, and no sharp transition is observed (below the order temperature) up to $\mu_0 H = 10\,T$, which is consistent with the absence of magnetic anisotropy. In contrast, other ANb_2O_6 systems, which present ferromagnetic chains, show pronounced spin-flip transitions [17,19].

3.3. Specific-heat measurements

The occurrence of a magnetic transition at low temperature for the $MnNb_{2-x}V_xO_6$ compounds was also checked through specific-heat measurements, carried out down to 1.8 K. For comparison, corresponding measurements were carried out in the isostructural non-magnetic compound $ZnNb_2O_6$, as shown in Fig. 7. Concentration dependence of the specific-heat behavior with temperature can be seen in the inset of that figure. All $MnNb_{2-x}V_xO_6$ samples present peaks near T_N, while $ZnNb_2O_6$ has no magnetic ordered state. The Néel temperatures are 4.40, 4.64 and 4.68 K for $x = 0.0$, 0.1 and 0.2, respectively. These values agree with those obtained by magnetic measurements. Similar values are reported in the literature [7,15,16].

3.4. Neutron diffraction

Neutron-diffraction measurements were done in the range 1.4–280 K. Rietveld refinement of the ND pattern ($\lambda = 2.52$ Å) recorded at 280 K for $MnNb_2O_6$ is shown in Fig. 8. Bragg positions correspond to the *Pbcn* space group. Fig. 9 shows the temperature dependence of the unit-cell parameters for $MnNb_2O_6$ as obtained from ND.

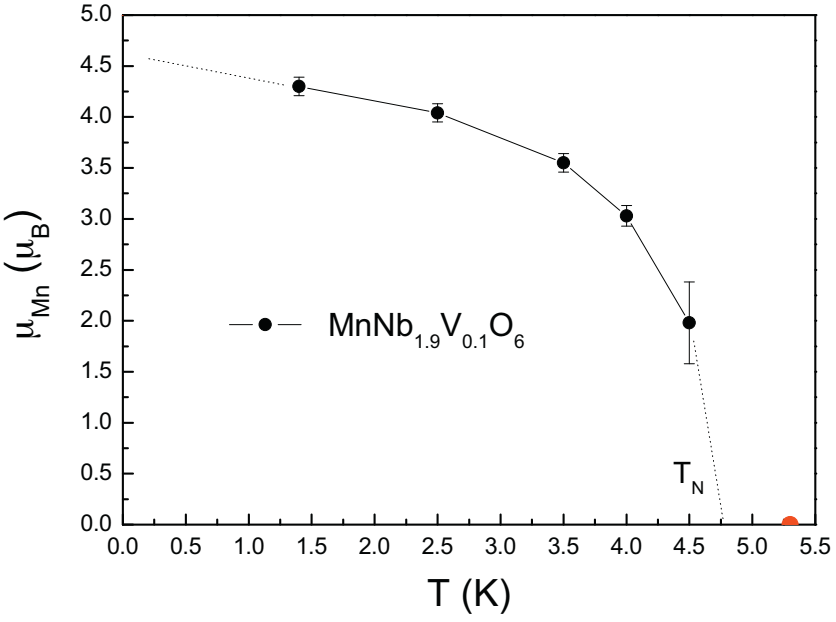

Fig. 12. Temperature dependence of Mn magnetic moment for $MnNb_{1.9}V_{0.1}O_6$ as obtained from the Rietveld refinement of the ND patterns.

For ND measurements taken at $T < T_N$ it is possible to observe peaks related to the magnetic structure. Fig. 10 shows the Rietveld refinement of the ND pattern recorded at 1.5 K for $MnNb_{1.8}V_{0.2}O_6$. The Bragg positions correspond to the *Pbcn* space group of the crystal structure and to the magnetic phase, as indicated. The magnetic structure is commensurable with the lattice at this temperature and presents a propagation vector $k = (0,0,0)$. A very small peak at about 16° corresponds to the largest magnetic peak from trace of C2/m variant of MnV_2O_6. The concentration of this phase was too low to be detected by X-ray diffraction and is only revealed by neutron diffraction. It has been estimated to 1 percent.

The cell parameters obtained in this work, both from XRD (Table 1) and ND (Table 4), are in agreement with the literature [6,7,15].

The magnetic moments are antiferromagnetically coupled along the *c* axis with an angle of 71° related to the same axis and Fig. 11 shows the configuration obtained by ND results. Unlike other divalent cations (Fe, Co, Ni) [5,17–19] which are featured by large anisotropy, the Mn^{2+} cations are not forming Ising type chains running along the zig-zag of tilted octahedra. The Mn magnetic moments are tilted away from the *c* axis ($\theta \approx 71°$), they are antiferromagnetically coupled to the following one along the zig-zag chain. This antiferromagnetic coupling along the chain is in contrast to the ferro-coupling previously reported between the Fe, Ni or Co near neighbors. Table 4 shows that polar angle θ does not change as *x* increase, in contrast, φ, the azimuthal angle presents a variation and for $x = 0.2$ it is almost zero degree. Due to the $S = 5/2$ state of Mn cation and the expected zero value of the orbital moment, low magnetocrystalline anisotropy is expected for the Mn^{2+} cations leading to essentially Heisenberg type chains. This result is in excellent agreement with our hypothesis of Heisenberg chains, used for the analysis of magnetic measurements discussed above. The observed antiferromagnetic ordering of the Mn cations along the chains bears witness to the negative sign of the J exchange parameter.

Mn magnetic moment temperature dependence for $MnNb_{1.9}V_{0.1}O_6$ is shown in Fig. 12. Mn^{2+} magnetic moment observed at 1.5 K (4.3 μ_B) is lower than the expected magnetic moment ($gJ = 5\ \mu_B$) due to covalence as is typical in insulating oxides [6]. Neutron diffraction measurement performed at 5.5 K shows no peak related to the magnetic structure and it is shown as a red point in the diagram.

4. Conclusions

We did a systematic study of $MnNb_{2-x}V_xO_6$ samples (with *x* varying in the range 0–0.4). For $x < 0.2$, samples presented a single phase of *Pbcn* symmetry. For $x > 0.3$ we observed also a minority of phase *C2/m* symmetry, the same structure as MnV_2O_6. Susceptibility lines present an abroad maximum followed by an inflection point (T_N) which characterizes low dimensional magnetic behavior. Curie–Weiss fitting gives a negative Weiss temperature that is a characteristic of antiferromagnetic interactions in paramagnetic region. M(H,T) vary linearly with no sharp transitions for an applied field up to 10 *T*. Order temperature obtained by specific heat measurements increases with V content according to susceptibility results. ND measurements show that Mn magnetic moments form antiferromagnetic zig-zag chains running along the *c* axis. Unlike other orthorhombic (Fe;Ni;Co)Nb_2O_6 systems that presents ferromagnetic Ising chains. At 1.5 K, the Mn atoms are found to carry an ordered magnetic moment of about 4.3 μ_B, the magnetic moment tilted away from the *c* axis (by $\theta \approx 71°$). The angle φ varies with V concentration, and decreases from about 10° to almost zero for $x = 0$ and 0.2 respectively. The Mn chains are antiferromagnetic and do not present significant anisotropy. These characteristics and the high spin allowed us to model the system as weakly interacting classical Heisenberg chains, estimating the values of intra- and interchain exchange constants. The intrachain is found to be $J = -1.09k_B$ in $MnNb_2O_6$ and the mean interchain exchange constant is quantified to $-0.365k_B$. V for Nb substitution is found to induce a cell contraction and consequently a progressive reduction of both the intra and interchain interactions.

Acknowledgments

Funding for this project was provided by a grant from Région Rhône-Alpes (MIRA scholarship). The present work was also supported by the Brazilian agency CNPq, and in part by the Brazilian-France agreement CAPES-COFECUB (No. 600/08).

References

[1] Y. Zhou, M. Lu, Z. Qiu, A. Zhang, Q. Ma, H. Zhang, Z. Yang, Photoluminescence of $NiNb_2O_6$ nanoparticles prepared by combustion method, Mater. Sci. Eng. B 140 (2007) 128–131.
[2] R.C. Pullar, C. Vaughan, N. McN Alford, The effects of sintering aids upon dielectric microwave properties of columbite niobates, $M^{2+}Nb_2O_6$, J. Phys. D 37 (2004) 348–352.
[3] R.C. Pullar, The synthesis, properties, and applications of columbite niobates ($M^{2+}Nb_2O_6$): a critical review, J. Am. Ceram. Soc. 92 (2009) 563–577.
[4] E.J. Kinast, V. Antonietti, D. Schmitt, O. Isnard, J.B.M. da Cunha, M.A. Gusmão, C. A. dos Santos, Bicriticality in $Fe_xCo_{1-x}Ta_2O_6$, Phys. Rev. Lett. 91 (2003) 197208.
[5] C. Heid, H. Weitzel, P. Burlet, M. Bonnet, W. Gonschorek, T. Vogt, J. Norwig, H. Fuess, Magnetic phase diagram of $CoNb_2O_6$: a neutron diffraction study, J. Magn. Magn. Mater. 151 (1995) 123–131.
[6] S.A.J. Kimber, J.P. Attfield, Disrupted antiferromagnetism in the brannerite MnV_2O_6, Phys. Rev. B 75 (2007) 064406.
[7] O.V. Nielsen, B. Lebech, F. Krebs Larsen, L.M. Holmes, A.A. Ballman, A neutron diffraction study of the nuclear and magnetic structure of $MnNb_2O_6$, J. Phys. C 9 (1976) 2401–2411.
[8] M.G.B. Drew, R.J. Hobson, V.T. Padayatchy, Synthesis, structure and magnetic properties of monoclinic $CuNb_2O_6$ and the electronic spectra of both polymorphs of $CuNb_2O_6$, J. Mater. Chem. 5 (1995) 1779–1783.
[9] Z. Chuan-Cang, L. Fa-Min, D. Peng, C. Lu-Gang, Z. Wen-Wu, Z. Huan, Synthesis, structure and antiferromagnetic behaviour of brannerite MnV_2O_6, Chin. Phys. B 19 (2010) 067503.
[10] C. Calvo, D. Manolescu, Refinement of the structure of CuV_2O_6, Acta Cryst. Sec. B 29 (1973) 1743–1745.
[11] R.W.G. Wyckoff, Crystal Structure, Wiley, New York, 1965.
[12] A.I. Zaslavsky, Y.D. Kondrashev, S.S. Tolkachev, Dokl. Akad. Nauk SSSR 75 (1950) 559.
[13] S. Kobayashi, S. Mitsuda, M. Ishikawa, K. Miyatani, K. Kohn, Three-dimensional magnetic ordering in the quasi-one-dimensional Ising magnet $CoNb_2O_6$ with partially released geometrical frustration, Phys. Rev. B 60 (1999) 3331–3345.
[14] C. Heid, H. Weitzel, P. Burlet, M. Winkelmann, H. Ehrenberg, H. Fuess, Magnetic phase diagrams of $CoNb_2O_6$, Phys. B 234 (1997) 574–575.
[15] L.M. Holmes, A.A. Ballman, R.R. Hecker, Antiferromagnetic ordering in $MnNb_2O_5$ studied by magnetoeletric and magnetic susceptibility measurements, Solid State Commun. 11 (1972) 409–413.
[16] D. Prabhakaran, F.R. Wondre, A.T. Boothroyd, Preparation of large single crystals of ANb_2O_6 (A = Ni, Co Fe, Mn) by the floating-zone method, J. Crys. Growth 250 (2003) 72–76.
[17] P.W.C. Sarvezuk, M.A. Gusmão, J.B.M. da Cunha, O. Isnard, Magnetic behavior of the $Ni_xFe_{1-x}Nb_2O_6$ quasi-one-dimensional system: Isolation of Ising chains by frustration, Phys Rev. B 86 (2012) 054435.
[18] P.W.C. Sarvezuk, E.J. Kinast, C.V. Colin, M.A. Gusmão, J.B.M. da Cunha, O. Isnard, New investigation of the magnetic structure of $CoNb_2O_6$ columbite, J. Appl. Phys. 109 (2011) 07E160.
[19] P.W.C. Sarvezuk, E.J. Kinast, C.V. Colin, M.A. Gusmão, J.B.M. da Cunha, O. Isnard, Suppression of magnetic ordering in quasi-one-dimensional $Fe_xCo_{1-x}Nb_2O_6$ compounds, Phys. Rev. B 83 (2011) 174412.
[20] J. Rodriguez-Carvajal, Recent advances in magnetic structure determination by neutron powder diffraction, Phys. B 192 (1993) 55–69.
[21] L.B. McCusker, R.B. Von Dreele, D.E. Cox, D. Louer, P. Scardi, Rietveld refinement guidelines, J. Appl. Crystallogr. 32 (1999) 36–50.
[22] M.E. Fisher, Relation between the specific heat and susceptibility of an antiferromagnet, Philos. Mag. 82 (1962) 1731–1743.
[23] N.W. Ashcroft, N.D. Mermin, Introduction to Solid State, Philadelphia Saunders College Publishing, United States of America, United States of America, 1976.
[24] F. García-Alvarado, A. Orera, J. Canales-Vázquez, J.T.S. Irvine, On the electrical properties of synthetic manganocolumbite $MnNb_2O_{6-\delta}$, Chem. Mater. 18 (2006) 3827–3834.
[25] M.E. Fisher, Magnetism in one-dimensional systems-the Heisenberg model for infinite spin, Am. J. Phys. 32 (1964) 343–346.